GEOMETRIC REFINEMENT OF LiDAR ROOF CONTOURS USING PHOTOGRAMMETRIC DATA AND MARKOV RANDOM FIELD MODEL

A. P. Dal Poz

Dept. of Cartography, São Paulo State University, R. Roberto Simonsen, 305, Presidente Prudente-SP, Brazil - aluir@fct.unesp.br

Commission IV, WG IV/3

KEY WORDS: Digital Photogrammetry, Building Reconstruction, Spatial Analysis, Topographic Mapping, Optimization, LiDAR

ABSTRACT:

In this paper, a methodology is proposed for the geometric refinement of LiDAR building roof contours using high-resolution aerial images and Markov Random Field (MRF) models. The proposed methodology assumes that the 3D description of each building roof reconstructed from the LiDAR data (i.e., a polyhedron) is topologically correct and that it is only necessary to improve its accuracy. Since roof ridges are accurately extracted from LiDAR data, the main objective is to use high-resolution aerial images to improve the accuracy of roof outlines. In order to meet this goal, the available roof polyhedrons are first projected onto the image-space. Then, the projected polygons and the straight lines extracted from the image are used to establish an MRF description, which is based on relations (relative length, proximity, and orientation) between the two sets of straight lines. The energy function associated with the MRF is minimized using a minimizing algorithm, resulting in the grouping of straight lines for each roof object. Finally, each grouping of straight lines is topologically reconstructed based on the topology of the corresponding LiDAR polygon projected onto the image-space. The preliminary results showed that the proposed methodology is promising, since most sides of the refined polygons are geometrically better then corresponding projected LiDAR straight lines.

1. INTRODUCTION

Data acquisition for mapping and GIS using photogrammetric techniques has traditionally been performed via the manual extraction of cartographic features from images of the terrain surface ranging in scale from 1:3000 to 1:90000 (Sowmya and Trinder, 2000). Although manual extraction is adequate in terms of accuracy and reliability, it is time-consuming and expensive. On the other hand, due to imperfections in the image acquisition phase and the scene complexity, feature extraction from imagery and LiDAR data is too complex to be fully automated.

Building extraction methodologies are very important in the context of spatial data capture and updating for GIS applications. These methodologies may be classified into three categories according to the kind of input data, i.e.: LiDAR-based methodologies, photogrammetrically-based methodologies, and LiDAR/photogrammetrically-based methodologies. An example of the first category is found in Rottensteiner et al. (2005), in which an algorithm for roof line delineation from LiDAR data is proposed. Basically, roof edges and roof ridges are derived separately and combined to form a consistent polyhedral model. Vosselman (1999) also described another approach for the reconstruction of buildings by polyhedron models from LiDAR data. Photogrammetrically-based methodologies have been proposed for over 20 years. For example, Fua and Hanson (1987) proposed a methodology for locating and outlining complex rectilinear cultural objects (buildings) in aerial images. In Shufelt (1997) is described the PIVOT (Perspective Interpretation of Vanishing points for Objects in Three dimension) system, which aims at automatically extracting building from a single image. More recently, Müller and Zaum (2005) proposed a methodology for building detection in aerial images. First a region-growing algorithm is used to segment the entire image and then the buildings and vegetations are separated by a classification

procedure based on a set of geometric and photometric features derived for each segmented region.

LiDAR/photogrammetrically-based methodologies seek to take advantage of the synergy between LiDAR data and imagery data. Basically, LiDAR-based techniques are superior in deriving building heights and in extracting planar roof faces and roof ridge lines, whereas photogrammetrically-based techniques are superior in extracting building roof outlines (Kaartinen et al., 2005). A few LiDAR/photogrammetrically-based methodologies are found in the literature. Haala and Brenner (1999) combined multispectral imagery and DEM (Digital Elevation Model) derived from LiDAR data for separating building from vegetation. In Sohn and Dowman (2003) buildings are firstly extracted from both Ikonos imagery and from DEM/LiDAR data and, then, the results obtained from both data sources are combined to remove inconsistencies. Vosselman (2002) combined LiDAR, plan view, and high-resolution aerial image data to automatically reconstruct 3D building. Basically, the plan view is used as reference to extract polyhedral building model from LiDAR data. The high-resolution aerial images are used to refine the roof boundaries.
In this paper, a methodology is proposed for the geometric refinement of LiDAR building roof contours using high-resolution aerial images and MRF models. MRF models have been increasingly used in image analysis because they enable the exploitation of the local statistical dependence of image features and also allow global optimization to be accomplished through iterative local computations. This makes sense particularly in the context of roof building extraction because it is not necessary that all straight lines interact with one another. Instead, only a few straight lines that are spatially close to one

another and with specific angular relations with one another need to interact. Using projected LiDAR roof contours and their error projections, the neighboring set of straight lines associated with each building roof can be further reduced. This paper is organized as follows. Section 2 presents the proposed methodology. The preliminary results are presented and discussed in Section 3. Finally, the paper is finalized in Section 4 presenting some conclusions and outlook.

2. METHODOLOGY

The proposed methodology comprises preprocessing steps, the establishment of the energy function (U(**x**)) based on an MRF model, the solution of the energy function by applying a minimization algorithm, and the completion of the detected straight lines´ groupings for reconstructing the refined image-space roof contours. In the following sub-sections, details on briefly described steps of the proposed methodology are described. However, it will be given considerable emphasis on basic MRF theory and on development of the energy function.

2.1 Preprocessing

The preprocessing steps mainly comprise the projection of the 3D roof contours onto the image-space and the extraction of the image straight lines that are nearby the projected LiDAR roof contours. The techniques used in these steps are well-known and, as such, only more general details are presented.

In order to project the 3D building roof contours onto the image-space, two basic steps are necessary. First, the collinearity equations are used, along with the exterior orientation parameters, to transform the roof contours into the photogrammetric reference system. Second, an internal camera model and the associated interior orientation parameters are used to add systematic errors and to transform the roof contours from the photogrammetric reference system to the LC-image coordinate system. The error projections are estimated in order to construct a registration error model.

The registration error model is a simple bounding box constructed around each projected LiDAR straight line, which enables the straight line extraction process to be focused only on limited regions of the image, avoiding the extraction of irrelevant information. There is a large amount of research in the literature in the subject of straight line extraction. Examples of methods are the Burns line detector (Burns et al., 1984) and the Hough transform based methods (Balard and Brown, 1982). The algorithm for straight line extraction is based on standard image processing algorithms and seems to be effective for the present application. First, the Canny operator is used to generate a binary map with thinned edges. Next, an edge linking algorithm is applied to the edge map for organizing the pixels that lie along edges into sets of edge contours. In order to extract the straight lines, the edge contours are approximated by polylines through the recursive splitting method (Jain et al., 1995). Very small straight lines (2-3 pixels length) and straight lines differing too much in orientation (e.g., 20^o) from the projected LiDAR roof contour are removed, since they are unlikely to be valid candidates for constituting roof contours. In the last step, simple perceptual grouping rules (i.e., proximity and collinearity) are used to merge collinear straight lines and then to further reduce the number of candidates for representing the roof contours.

2.2 MRF concepts and the energy function

2.2.1 Basic concepts of the MRF theory

MRF theory provides an efficient way to model context-dependent features such as straight lines forming a roof building contour. In an MRF, the sites in S= {1, …, n} are related to one another through a neighborhood system defined as N= {N_i, i ∈ S}, where N_i is the set of sites neighboring i. A random field *X* is said to be an MRF on S with respect to a neighborhood system N if and only if,

$$P(\mathbf{x}) > 0,\ \forall_x \in \mathbf{X}$$
$$P(x_i \mid x_{S-\{i\}}) = P(x_i \mid x_{N_i}) \quad (1)$$

Note that **x** is a configuration of *X* and **X** is the set of all possible configurations. Also note that $x_i \in \mathbf{x}$ and $x_{S-\{i\}}$ (or $x_{N_i}) \subset \mathbf{x}$. As stated by the Hammersley-Clifford theorem, an MRF can also be characterized by a Gibbs distribution (Kopparapu and Desai, 2001), i. e.,

$$P(\mathbf{x}) = \frac{\exp(-U(\mathbf{x}))}{Z} \quad (2)$$

where:

$$Z = \sum_{\mathbf{x} \in \mathbf{X}} \exp(-U(\mathbf{x})) \quad (3)$$

is a normalizing constant and U(**x**) is an energy function, which can be expressed as:

$$U(\mathbf{x}) = \sum_{c \in C} V_c(\mathbf{x}) \quad (4)$$

Equation 4 shows that the energy function is a sum of clique potentials (V_c(**x**)) over all possible cliques c ∈ C. A clique c is a subset of sites in S in which every pair of distinct sites are neighbors. The value of V_c(**x**) depends on the local configuration on clique c. For more detail on MRF and Gibbs distribution see e.g. Kopparapu and Desai (2001) and Modestino and Zhang (1992).

2.2.2 The energy function:

Straight lines resulting from the image processing techniques are used to construct an MRF model expressing the specific shapes of building roofs, having as reference the polygons resulted from the photogrammetric projection of LiDAR roof contours. The associated energy function is defined in such way that each straight line is associated with a discrete random variable (x_i) assuming binary values according to the following rule:

$$x_i = \begin{cases} 1 & \text{iff the } i^{th} \text{ straight line} \\ & \text{belongs to a roof contour;} \\ 0 & \text{otherwise.} \end{cases} \quad (5)$$

The above rule gives rise to an n-dimensional discrete random vector, where n is the number of straight lines to be considered in the optimization process. This random vector is the unknown in the optimization process. Theoretically, the search space has 2^n combinations to be considered in the global minimum computation of the energy function. The optimization algorithm used will be described later.

Before proceeding with the development of the energy function, it is necessary to define two metrics, called the proximity and orientation metrics. Both metrics are the basis for defining the neighbour system for the problem under consideration.

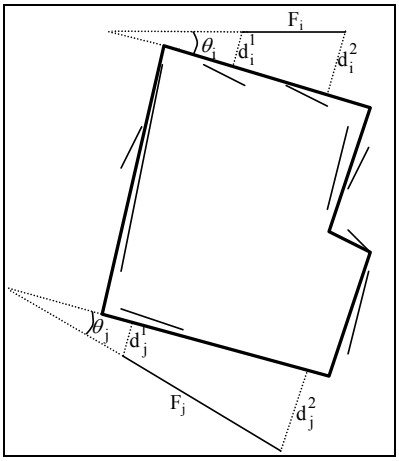

Figure 1. Geometric elements for defining the proximity and orientation metrics

The metric for the proximity between two straight lines F_i and F_j is defined as follows,

$$P(i, j) = \frac{1}{2}(d_i^1 + d_i^2 + d_j^1 + d_j^2) \quad (6)$$

where: d_i^1 and d_i^2 are the distances between the endpoints of the straight line F_i and the projected LiDAR straight line that is nearest to F_i

d_j^1 and d_j^2 are the distances between the endpoints of the straight line F_j and the projected LiDAR straight line that is nearest to F_j

Equation 6 is based on the principle that straight lines that are somehow interrelated and near to one another are perceived as belonging to a same unit. In this case, the unit is the reference roof contour, i.e., the projected LiDAR roof contour. The equation 6 is then an indirect proximity measurement between F_i and F_j, since it explicitly expresses the nearness between a pair of straight line (F_i and F_j) and the projected LiDAR roof contour. But, one can interpret that if both F_i and F_j are closed to the unit, then they are somehow near. It is also easy to note that the following properties hold: $P(i, j) \geq 0$ and $P(i, j) = P(j, i)$. In particular, $P(i, j) = 0$ if only if both straight lines (F_i and F_j) superpose the like parts of the projected LiDAR roof contour.

The metric for the orientation between two straight lines F_i and F_j follows the same principles of the proximity metric and it is defined tanking into account the sigmoid function, i.e.,

$$s_\theta(i, j) = \frac{2}{1 + \exp[-\beta.(\theta - \theta_o)^2]} - 1 \quad (7)$$

where: $\theta = \theta_i + \theta_j$

θ_i is the angle between the straight line F_i and the projected LiDAR straight line that is nearest to F_i

θ_j is the angle between the straight line F_j and the projected LiDAR straight line that is nearest to F_j

β is a positive constant

θ_o is the optimal value (0^o or 180^o) of the parameter θ

The sigmoid function has some interesting properties: 1) it has only a minimum point at $\theta = \theta_o$; 2) it takes value over [0; 1]; 3) it is symmetric around $\theta = \theta_o$; and 4) the constant β can be used to control the shape of the sigmoid function. The larger is the parameter β, the harder is the penalization of deviations of θ from θ_o.

Now, if N_i is the set of sites neighboring i, then any site $j \in N_i$ if only if,

$$\begin{cases} P(i, j) \leq t_P \\ s_\theta(i, j) \leq t_s \end{cases} \quad (8)$$

where: t_p and t_s are the proximity and orientation thresholds, respectively

The energy function $U(\mathbf{x})$ is elaborated based on three energy terms. The first term is an one-site click energy defined in such way to favor longer straight line, taking as reference the nearest projected LiDAR straight line. This energy term ($U_1(\mathbf{x})$) is expressed as follows,

$$U_1(\mathbf{x}) = \sum_{i=1}^{n} x_i \frac{L^L_{F_i}}{L_{F_i}} \quad (9)$$

where: n is the number of image straight lines

$L^L_{F_i}$ is the length of the projected LiDAR straight line that is nearest to the i^{th} image straight line (F_i)

L_{F_i} is the length of the i^{th} image straight line (F_i)

The second term is a two-site click energy that favors straight lines that are nearer to the projected LiDAR roof contour. This term is called the proximity energy term and is formulated as follows,

$$U_2(\mathbf{x}) = \frac{\sum_{i=1}^{n} \sum_{j \| j \in N_i} x_i . x_j . P(i,j)}{\sum_{i=1}^{n} x_i . (\sum_{i=1}^{n} x_i - 1)} \quad (10)$$

The third term is also a two-site click energy and it supports straight lines that have similar orientations in relation to the projected LiDAR roof contour. This term is called the orientation energy term and is formulated as follows,

$$U_3(\mathbf{x}) = \frac{\sum_{i=1}^{n} \sum_{j \| j \in N_i} x_i . x_j . s_\theta(i,j)}{\sum_{i=1}^{n} x_i . (\sum_{i=1}^{n} x_i - 1)} \quad (11)$$

The energy function can be finally expressed as follows:

$$U(\mathbf{x}) = \alpha_1 . U_1(\mathbf{x}) + \alpha_2 . U_2(\mathbf{x}) + \alpha_3 . U_3(\mathbf{x}) \quad (12)$$

where: α_1, α_2, and α_3 are positive constants.

The second and third terms of energy have in the denominator the term $\sum_{i=1}^{n} x_i > 1$. This means that each configuration needs to allow at least two correspondences. The optimal configuration ($\mathbf{x_{opt}}$) is obtained by minimizing the energy function, i.e., $\mathbf{x_{opt}}$= argmin($U(\mathbf{x})$). The minimization problem will be discussed in the next section.

2.3 Solution of the energy function

In order to obtain the optimal configuration ($\mathbf{x_{opt}}$) it is necessary to find the global minimum of the energy function ($U(\mathbf{x})$). The global minimum can be found by the so-called brute force searching method. This method is a simple and general problem-solving technique, which consists of exhaustively searching for the best candidate among all possible configurations. It is simple to implement and, if a solution exists, it always finds it. The great problem of using the brute force method is that in many practical problems the number of candidates can be so large that the problem becomes intractable. In general, the brute force method can be used when the problem complexity is relatively simple or when there are problem-domain heuristics that can allow the search space size to be reduced properly. In the sequence, it will be showed that the problem in hand can be transformed into a tractable one, even when the complexity of the building is relatively high.

In order to avoid the combinatorial explosion associated with the problem in hand, two constraints are used:

1) Uniqueness constraint: each projected LiDAR straight line must have at most one correspondence, which is either an image straight line or no entity. This means that $\sum_{i=1}^{n} x_i \le m$, where m is the number of projected LiDAR straight lines. Let n_1, n_2, …, n_m be the number of straight lines that are nearby the corresponding projected LiDAR straight lines. It is easily noted that $n = n_1 + n_2 + \ldots + n_m$. The number of configurations that needs to be checked is $C_1 = (n_1 + 1).(n_2 + 1) \ldots (n_m + 1) << |\mathbf{X}| = 2^n$.
2) Minimum-expected correspondences´ constraint: It is reasonable to expect a minimum of correspondences for the problem in hand. Assuming a p percent rate, the configurations **x** to be checked need to respect the following restriction: $int(m?) \le \sum_{i=1}^{n} x_i \le m$, where $m? = p.m/100$ and int(**a**) means the near integer of **a**, such that $int(\mathbf{a}) \le \mathbf{a}$. Now assuming for simplicity $n_1 = n_2 = \ldots = n_m = n´$, the number of configurations is $C_2 = \left[\binom{m}{m?} + \binom{m}{m?+1} + \ldots + \binom{m}{m-1}\right].n?^2 + 2^m << C_1$.

The brute force search method modified with the two domain constraints described above is called *constrained brute force search method*. In order to demonstrate that the two domain constraints can reduce the search space to a tractable size, an example considering a relatively complex building with 20-side roof contour (m= 20) is analysed. Usually, the proposed preprocessing techniques extract 1-3 straight lines around each projected LiDAR straight line. Tanking into account an average extraction of two straight lines around each projected LiDAR straight line, the following holds: 1) n= 40; 2) $n_1 = n_2 = \ldots = n_{20} = n´ = 2$; 3) $|\mathbf{X}| = 2^n = 1{,}099{,}511{,}627{,}776$; 4) $C_1 = 3{,}486{,}784{,}401$ (~99,7% reduction); 5) $C_2 = 1{,}048{,}786$ (p= 90), which is a reduction of about 99,9996% when compared to the number of candidates resulted from the uniqueness constraint. In other words, it is true that $C_2 << C_1 << |\mathbf{X}| = 2^n$.

2.4 Building contour completion

The optimisation method generates isolate image straight lines, whose one-to-one correspondences to the projected LiDAR straight lines are known. Projected LiDAR straight lines having no correspondences are kept together the matched image straight lines. Thus, the problem to be solved consists of the corner determination by line intersection. This is a simple problem because the topology of the projected LiDAR roof contour can be used to identify adjacent straight lines.

3. EXPERIMENTAL RESULTS

The test data consists of a high-resolution aerial image and a 3D bulding model generated automaticaly and previously by a preexisting methodology that processes LiDAR point clound. The test area is located in the city of Curitiba, Brazil. The image has 4500 pixels x 3000 pixels and the pixel footprint is about 20 cm. The interior orientation parameters of the camera and also the exterior orientation parameters of the images are known. Figure 2 shows the test building used in the preliminary experiment. This is an (inverted) E-shaped building, with a 19-side roof contour. Please note that some slight shadowed roof faces have low contrast with the background and, as a result, their edges are not well-defined.

Figure 2. Test building

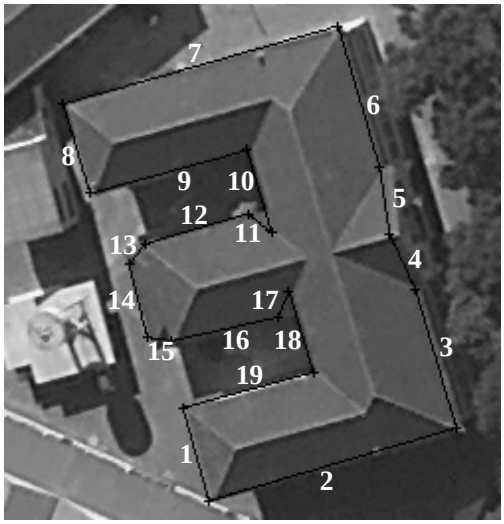

Figure 3. Projected LiDAR straight lines

Figure 3 shows the projected LiDAR straight lines obtained through the projection of the 3D roof contour. The resulting polygon is relatively close to the building roof edges, as a small registration error of about 5-pixel maximum is present. This largest registration error occurs with the LiDAR straight line 5. However, the LiDAR straight lines 13 and 15 do not aproximate correctly the details that are nearby them.

Figure 4 shows that twenty-four straight lines are extracted by the preprocessing steps. The projected straight lines have the following number of candidate for matching: ten projected straight lines have only one candidate; seven projected straight lines have two candidate; and two straight lines have no candidates. This result shows that the preprocessing steps filter out irrelevant information properly. Straight lines that are successfully matched to the projected LiDAR roof contour are overlaid in white on the image. The remaining straight lines that are rejected by the matching process appear in black. As shown in figure 4, the methodology found fourteen (74%) correspondences, in which thirteen (69%) are correct and one (5%) is incorrect (false positive). Please note that the incorrect matching occurred because the matched straight lines is nearer to the projected LiDAR straight line 5 than the another candidate for matching. In addition, both candidates for matching have similar length and orientation related to the projected LiDAR straight line 5. Figure 4 also shows that the methodology did not find five (26%) correspondences (false negatives). All false negative cases are related to either the absence of candidates (i.e., the nearby LiDAR straight lines 11 and 17) or the presence of invalid candidates (i.e., the nearby LiDAR straight lines 4, 13, and 15).

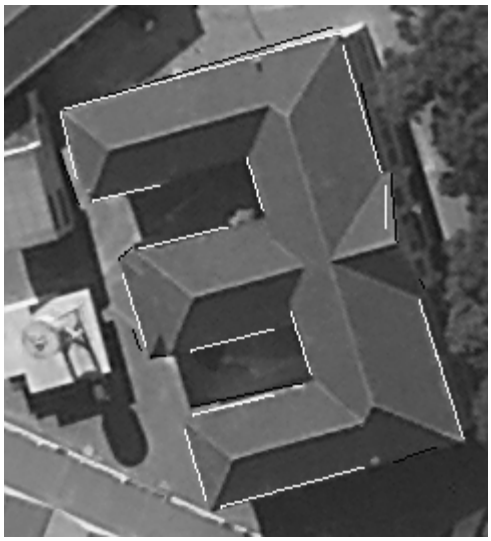

Figure 4. Matching result

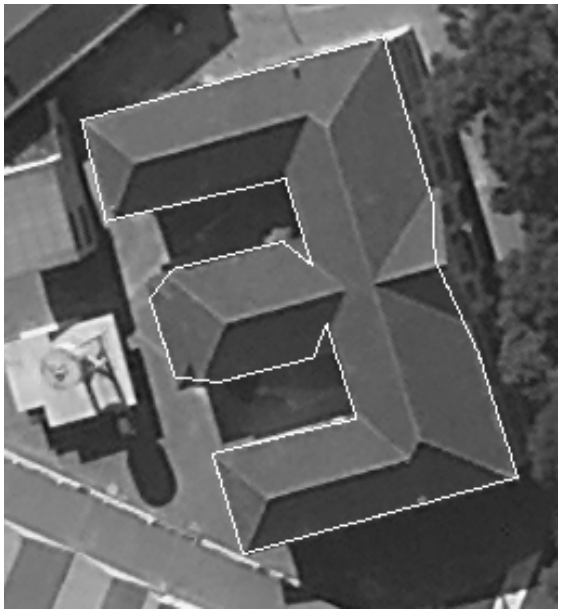

Figure 5. Completion result

Figure 5 presents the result of the proposed completion strategy. Fourteen projected LiDAR straight lines are replaced by the matched straight lines. These straight lines are potentially better representations for the corresponding projected LiDAR straight lines. The projected LiDAR straight lines 4, 11, 13, 15, and 17 are kept because they do not have correspondences among the straight lines extracted by the preprocessing steps. The refined image-space roof contour is determined by using the new straight line grouping constructed through the above rules, along with the topology of the projected LiDAR roof contour polygon. Basically, the new image-space roof contour polygon

vertices are determined by accomplishing the intersection between adjacent straight lines, according to the topology of the projected LiDAR roof contour polygon. The final result is better than the projected LiDAR polygon because most parts of the refined polygon are improved to some degree. The proposed methodology was not able to provide satisfactory results along four sides of the refined polygon. The roof gable defined by the straight lines 4 and 5 remains with a poor geometric description. The reasons for this poor results are twofold: 1) the deficiency of the proposed approach in finding the correct matching for the projected LiDAR straight line 5; and 2) the lack of a valid candidate for the projected LiDAR straight line 4. The roof details neighboring the straight lines 13 and 15 were poorly described due to a basic reason. The geometric descriptions of the corresponding parts of the polyhedron extracted from the 3D laser data are not enough to be handled by the proposed approach properly. Finally, based on the above analysis, the completeness and correctness of the result are 100% and 79% ($\cong$ 15/19), respectively.

4. CONCLUSIONS AND OUTLOOK

In this paper a methodology was proposed for geometric refinement of LiDAR roof contour project onto the image-space. An MRF description for groupings of image-space roof contour straight lines was developed, assuming that each building roof contour reconstructed from the LiDAR data is topologically correct, but its geometry needs to be improved. The MRF description is formulated based on relations (length, proximity, and orientation) between straight lines extracted from the image and the projected roof contour polygon. The groupings of straight lines are obtained by optimizing an energy equation associated to the MRF description. The topology of the projected LiDAR roof contour is used to get the polygon representing the refined image-space roof contour.

The preliminary results showed that the proposed methodology is promising. Although only a test was presented and discussed, it involves a building with a relatively complex geometry and a low contrast with the background. Most sides of the refined polygon are geometrically better then corresponding projected LiDAR straight lines. The general quality of the obtained result can be expressed by the completeness and correctness parameters, which were 100% and 79%, respectively.

Some directions for future developments are the improvements of the energy function and the use of more appropriate optimization methods (as, e.g., the simulated annealing algorithm) of the energy function, mainly to allow high-dimensional problems to be treated properly. The energy function can be improved tanking into account the shadow information, the corner information, the laser heights, besides other cues.

ACKNOWLEDGEMENTS

This paper was carried out with support of CNPq, National Council for the Scientific and Technological Development – Brazil, and FAPESP, São Paulo State Foundation for Research Development - Brazil. The available building polyhedron model used in the experiment was previously extracted from LiDAR data supplied by LACTEC – Technological Institute for Development, Brazil.

REFERENCES

Ballard, D. H.; Brown, C. M., 1982. *Computer Vision*. Prentice Hall, Inc., Englewood Cliffs, New Jersey, 523p.

Burns, J. B.; Hanson, A. B.; Riseman, E. M., 1986. Extracting straight lines. *IEEE Transactions on Pattern Analilysis and Machine Intelligence*, 8(4), pp. 425-455.

Fua, P.; Hanson, A. J., 1987. Resegmentation using generic shape: Locating general cultural objects. *Pattern Recognition Letters*, 5, pp. 243-252.

Haala, N.; Brenner, C., 1999. Extraction of buildings and trees in urban environments. *ISPRS Journal of Photogrammetry and Remote Sensing*, 54, pp. 130-137.

Jain, R.; Kasturi, R.; Schunck, B.G., 1995. *Machine Vision*. MIT Press and McGraw-Hill, New York, 549p.

Kaartinen, H.; Hyyppä, J.; Gülch, E.; Vosselman, G. et al., 2005. Accuracy of the 3D city model: EuroSDR comparison. In: The *International Archives of the Photogrammetry, Remote Sensing and Spatial Information Sciences*, Enschede, The Netherlands, Vol. XXXVI,, pp. 227-232.

Kopparapu, S. K.; Desai, U. B., 2001. *Bayesian approach to image interpretation*. Springer, 127p.

Modestino, J. A; Zhang, J. A., 1992. Markov Random Field model based approach to image interpretation. *IEEE Transactions on Pattern Analysis and Machine Intelligence*, 6, pp. 606-615.

Müller, S.; Zaum, D. W., 2005. Robust building detection in aerial images. In: The *International Archives of the Photogrammetry, Remote Sensing and Spatial Information Sciences*, Vienna, Austria, v. XXXVI, pp. 143-148.

Rottensteiner, F.; Trinder, J.; Clode, S.; Kubik, K., 2005. Automated delineation of roof planes from LIDAR Data. In: The *International Archives of the Photogrammetry, Remote Sensing and Spatial Information Sciences*, Enschede, The Netherlands, Vol. XXXVI, pp. 221-226.

Shufelt, J. A., 1997. Geometric constraints on hypothesis generation for monocular building extraction. In: *SPIE – Conference Integrating Photogrammetric Techniques with Scene Analysis and Machine Vision III*, Orlando, USA, Vol. 3072.

Sohn, G.; Dowman, I. J., 2003. Building extraction using Lidar DEMs and Ikonos images. In: The *International Archives of the Photogrammetry, Remote Sensing and Spatial Information Sciences*, Dresden, Germany, Vol. XXXIV.

Sowmya, A; J. C. Trinder, 2000. Modelling and representation issues in automated feature extraction from aerial and satellite images. *ISPRS Journal of Photogrammetry and Remote Sensing*, 55(1), pp. 34-47.

Vosselman, G., 1999. Building reconstruction using planar faces in very high density height data. In: *The International Archives of the Photogrammetry, Remote Sensing and Spatial Information Sciences*, Munich, Germany, Vol. XXXII, pp. 87-92.

Vosselman, G., 2002. Fusion of Laser Scanning Data, Maps, and Aerial Photographs for Building Reconstruction. In: IEEE *International Geoscience and Remote Sensing Symposium*, Toronto, Canada, CD-ROM (4 pages).